8th ECCOMAS Thematic Conference on the Mechanical Response of Composites
COMPOSITES 2021
M. Fagerström & C. Catalanotti (Editors)

Modelling damage growth in composites using a unified physically-based finite deformation model

Sérgio Costa[1,*], **Miguel Herraez**[2], **Hana Zrida**[3], **Robin Olsson**[1], **Rickard Östlund**[3]

[1] RISE SICOMP AB, Box 104, SE-431 22 Mölndal, Sweden.

[2] Materials Science and Engineering Area, University Rey Juan Carlos, c/Tulipán s/n, Móstoles, 28933, Madrid, Spain.

[3] Gestamp Hardtech AB, Luleå, Sweden.

[*] sergio.costa@ri.se

Keywords: Modelling damage, Experimental validation, Industrial applications.

Abstract

A 3D mesoscale model for damage growth is unified. The fibre kinking behaviour is based on fibre kinking theory handled in a finite deformation framework. The nonlinear shear behaviour is pressure dependent and is modelled by combining damage and friction on the fracture plane. Fibre kinking growth and transverse behaviour are mutually influenced and modeled with a single damage variable. This allows both modes to occur simultaneously in an efficient and physically-based way. For verification the model is tested against micro-mechanical FE simulations and against selected component tests. The combination of both models results in a high definition and physically-based 3D constitutive model for damage growth and crushing of composite materials.

1. Introduction

The use of composite materials in automotive structural components is challenging due to material and design costs arising from extensive testing necessary to ensure crashworthiness [1]. Therefore, predictive crash models are necessary to shorten the design cycle and thus reduce costs of using composites more competitively by replacing more expensive tests with cheaper simulation.

In order to help in designing composite materials, several models with focus on failure and damage have been proposed in the literature, e.g. [18, 13]. There are also models directed towards crash applications such as [20, 14, 7].

Despite significant progress, there is no clear superiority among the models in capturing progressive failure and crash with high fidelity.The complexity with damage modeling arises partly from the interaction of the different mechanisms for a varying stress state. Approaches that lock the damage modes [20, 6, 19], or that let the damage modes interchange between themselves oversimplify the physical complexity.

The present model results from extensive efforts in combining the complex physics of damage growth of composite materials into a single model capable of predicting the intralaminar

damage mechanisms and their interaction. The model is based on Continuum Damage Mechanics (CDM), i.e. there is a damage variable accounting for the type and/or distribution of damage mechanisms at the ply level.

The behaviour in fibre tension is dictated by the fibres and not affected by other stress states. Therefore, no interaction is considered between the damage modes. However, damage during compression along the fibres is in fact matrix damage meaning that the transverse response will be weaker. In a similar fashion, damage during transverse or shear load will degrade the longitudinal compressive response. This approach give the model the flexibility to interact between damage modes dominated by shear. For example matrix damage in shear, compression, matrix tension and fibre compression are modeled with a single damage variable.

The nonlinear shear behaviour combines damage and friction as first used in composite materials by [11] and later improved and validated for a 45 degree arrow shaped specimen by [7]. The fibre kinking behaviour is modelled in a novel way. The shear rotation of the fibres is computed based on finite deformation approaches [8], thus saving computational efforts compared to previous models [10, 9]. The fibres are assumed to inherit an initial misalignment. Under transverse compression this misalignment has negligible influence on the behaviour. However, under longitudinal compression, the initially misaligned fibres rotate further causing the matrix to yield. These complex mechanisms are merged into a single model in a simple and physically sound approach.

2. Model description

2.1 Constitutive relations in a finite deformation framework

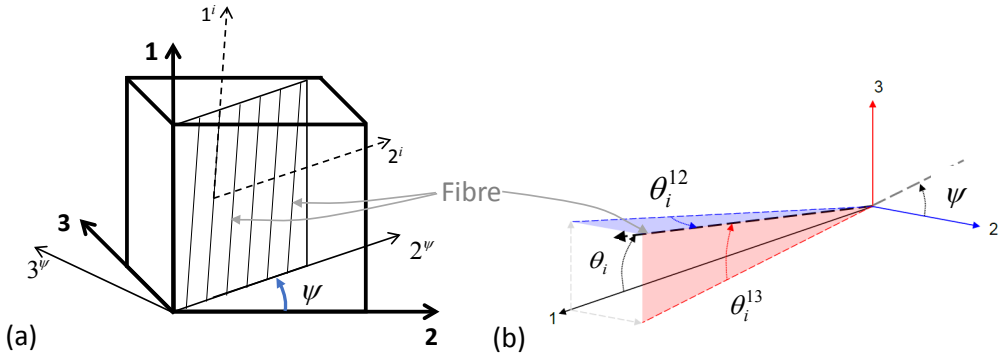

Figure 1. Illustration of: (a) 3D kink-band plane resulting from in-plane and out-of-plane misalignment [17]; (b) Definition of initial fibre misalignment (adapted from Ref. [2]).

Finite deformation theory is fundamental for the current constitutive model. In this section we will go through the fundamental constitutive equations of the model. Starting with the Green-Lagrange (G-L) strain, $\mathbf{E}$, is thus calculated as :

$$\mathbf{E} = \frac{1}{2}(\mathbf{F}^{\mathsf{T}}\mathbf{F} - \mathbf{I}) \tag{1}$$

where $\mathbf{F}$ is the deformation gradient and $\mathbf{I}$ is the second order identity tensor. Once the kink-band plane is obtained, the G-L strain tensor components can be transformed from the global coordinate system to the the kink-band plane, ψ, as shown in Fig. 1. The transformation is (on matrix form) given by:

$$\mathbf{E}^{\psi} = \mathbf{T}_{\psi}\mathbf{E}\mathbf{T}_{\psi}^{T} \tag{2}$$

where $\mathbf{T}_{\psi}$ is the transformation matrix for a rotation around the 1-axis with an angle ψ. The aim is to model the nonlinear shear response in the material frame, therefore, the strain tensor components need to be further transformed into the 'misaligned' frame as:

$$\mathbf{E}^{\psi,i} = \mathbf{T}_{i}\mathbf{E}^{\psi}\mathbf{T}_{i}^{T} \tag{3}$$

where $\mathbf{T}_i$ is the transformation matrix for rotation with an angle θ_i (around the 3^{ψ}-axis).

The constitutive response in the material coordinate system is then given by

$$\mathbf{S}^{i,\psi} = \mathbf{C}\mathbf{E}^{i,\psi} \tag{4}$$

where $\mathbf{S}^{i,\psi}$ is the stress tensor and $\mathbf{C}$ is the stiffness tensor in the material coordinates.

2.2 Final failure

For increasing shear strains the shear stress and damage parameter increase monotonously until the strain reaches an experimentally determined critical strain. An experimentally based condition for final failure strain is introduced to represent fully-developed macroscopic cracks as follows:

$$fi^{ff} = \left(\frac{\gamma_L}{\gamma_L^{cr}}\right)^2 + \left(\frac{\gamma_T}{\gamma_T^{cr}}\right)^2 \tag{5}$$

where γ_L^{cr} is the shear strain at specimen rupture, γ_T^{cr} is obtained from transverse compression tests (already performed for material characterization). Using this failure condition the toughness measurements can be avoided. Once the final failure criterion is reached, the shear microcracks coalesce unstably into a macroscopic crack and the damage parameter rapidly reaches unity. The remaining low shear stress is caused by the frictional forces on the fracture surface. A steep strain softening behaviour results in growth of localized strains [3], which may cause oscillations and nonphysical response given that an explicit solver is used. This may result in numerical oscillations, excessive element distortions and slow down the simulation. Thus, a more robust method is necessary that does not cause instabilities and still captures the rapid degradation.

The proposed method for this rapid transition phase does not rely on physics which may be a reasonable simplification since this steep response has very low contribution to the energy

absorption. The proposed method consists of driving the damage variable by the "totaltime" variable rather than using a strain-driven damage. This approach avoids the pathological mesh distortions resulting from sudden localization of high strains since all elements experience the same "totaltime". When the final failure criterion in Eq. 5 is reached the damage variable d is redefined as:

$$d = 1 - \left(1 - d^0\right)\left(1 + \delta\gamma - t/t_0\right)/\delta\gamma \,, \tag{6}$$

where d^0 and t_0 are the damage and the simulation time at the onset of ply rupture, and $\delta\gamma$ is the variation of γ on the x–axis. In Eq. 6 the catastrophic failure progresses rapidly in order to have negligible influence on energy absorption. Therefore, d^0 it is kept within 2% of t_0, i.e. $\delta\gamma = 0.02$. A sensitivity study was performed and it was shown that for values of $\delta\gamma$ between 0.02 and 0.05 the simulation is stable and that no significant variations are observed in the crushing response [7].

2.3 Compute the fracture plane

The stresses on potential fracture planes are obtained from the constitutive response in the material coordinate system. The fracture plane if found by testing a failure criterion for several incremental angle. Once the failure criterion reaches unity at a given angle, it is fixed through the damage growth and the shear stress components acting on the fracture plane, $\mathbf{S}_L$ and $\mathbf{S}_T$, as shown in Fig. 2, drive the damage growth [11].

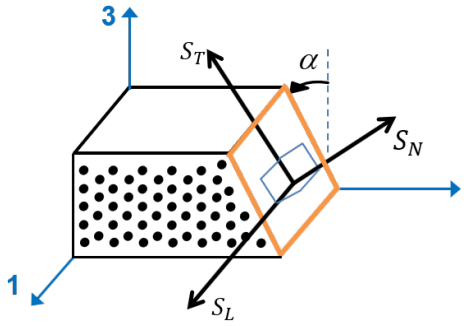

Figure 2. Second Piola-Kirchoff stresses on the fracture plane expressed in the NLT system

The components of the second Piola-Kirchoff stress tensor expressed in a coordinate system aligned with the ψ-plane, $\mathbf{S}^\psi$ are transformed as:

$$\mathbf{S}^\psi = \mathbf{T}_i^T \mathbf{S}^{i,\psi} \mathbf{T}_i \tag{7}$$

where T_i is the transformation matrix for the angle θ_i. Finally, for obtaining the global response, the stress tensor needs to be expressed in the global frame according to:

$$\mathbf{S} = \mathbf{T}_\psi^T \mathbf{S}^\psi \mathbf{T}_\psi \tag{8}$$

2.4 Remaining damage modes

In order to put together a complete constitutive model for damage growth all the possible load cases need to be considered. In the previous sections we described the fibre kinking formation and the matrix cracking. In this section, we will show how these two mechanisms will be put together to account for all the damage modes as shown in Fig. 3. Notice that only two damage variables (matrix damage and fibre damage) are used for the whole model, thus, simplifying the modelling. This simplification reduces the number of equations which leads to lower number of mathematical operations necessary for the model. This simplification arguably captures the most important interactions in the matrix dominated damage modes. For example, fibre compression may lead to matrix cracking which will influence the transverse and shear behaviour. Therefore, it is difficult to justify the usage of additional damage variables. Possibly, this will be investigated further. A flowchart of the model with the interaction of the different damage modes is shown in Fig. 4.

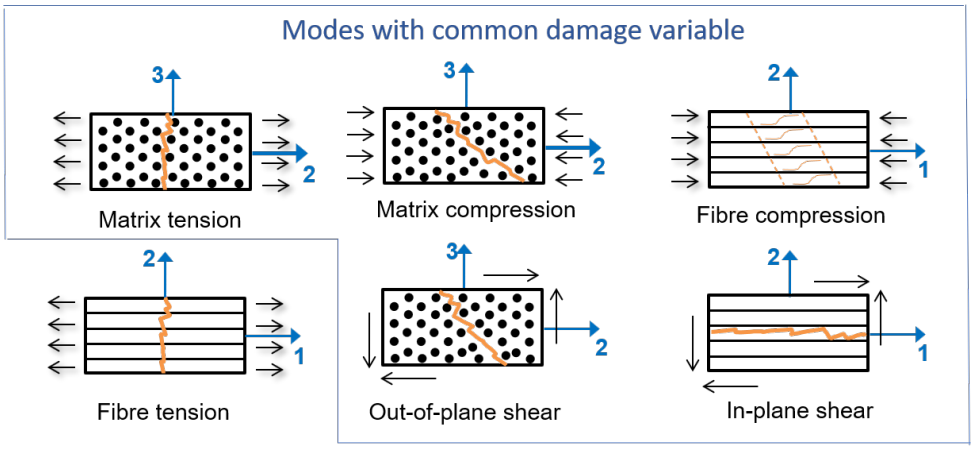

Figure 3. Damage modes

2.5 Material properties and model calibration

The material properties used in the simulations are shown in Table 1. The damage parameters are p (calibrated from the shear stress-strain curve), γ_0 is the shear strain at onset of damage ($\gamma_0 = \tau_0/G_{12}$) and γ_f is the shear strain at final decohesion. The friction parameters are the coefficient of friction on the micro-crack surfaces μ, and the internal pressure p_0. Note the lack of transverse compressive strength properties except the onset of nonlinearity in the shear response, τ_0. This value is defined visually from the beginning of shear nonlinearity in the shear response and is only used to obtain γ_0. The in-plane and out-of-plane fibre misalignments are represented by θ_i^{12} and θ_i^{13} respectively. Note that θ_i^{12} is assumed to be zero for simplicity but could take any value.

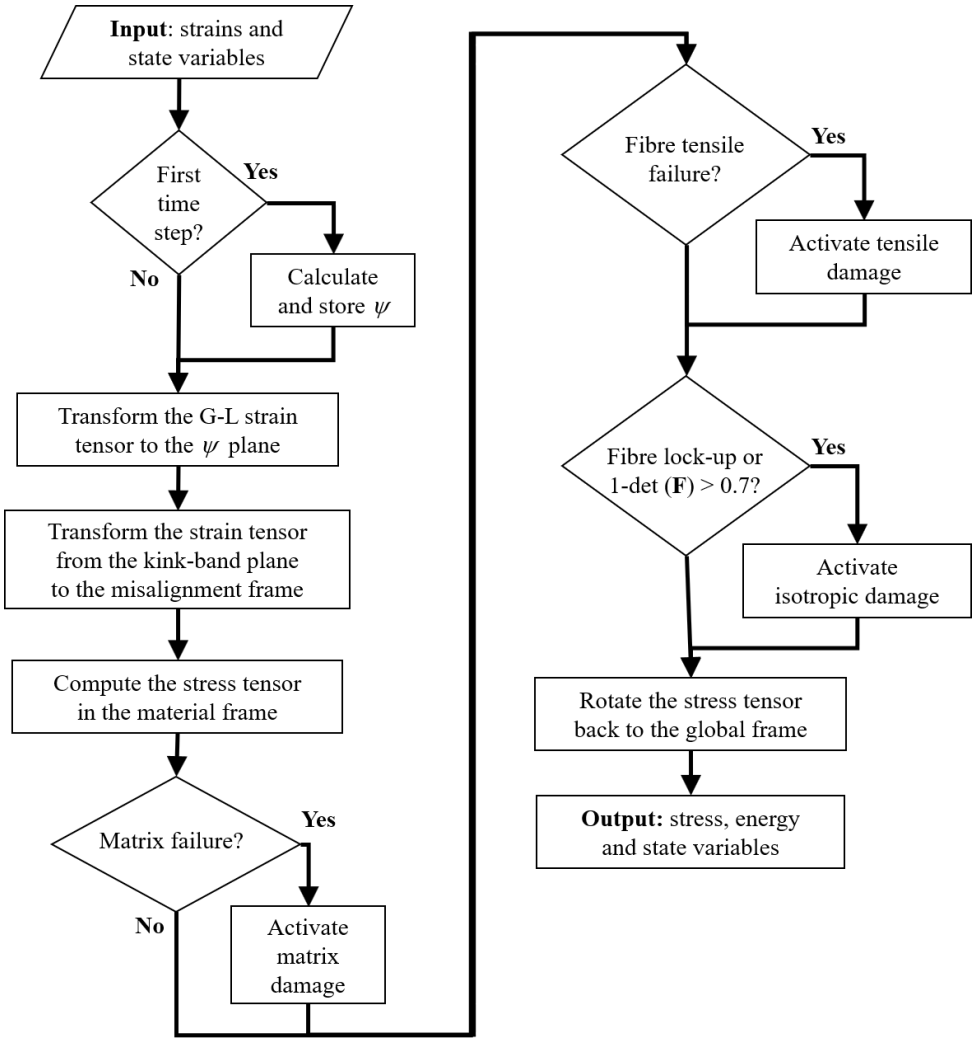

Figure 4. Flowchart of the model

From the material characterization side it is advantageous to have the full curve for the nonlinear shear behaviour with loading-unloading cycles. The unloading-loading response allows us to separate the material damage from other degrading mechanisms such as the viscoplasticty of the matrix. This contributes perhaps for a more informed choice of parameters driving the damage. The calibration is done by matching the nonlinear behaviour of the model with the test. Further calibration regarding the choice of the friction parameters that influence the pressure dependency behaviour are recommended but not required for most applications.

In the current work, the in-plane shear response of the model is calibrated against the experimental results obtained using the Iosipescu shear tests specimen, similarly to in [4]. The results of the calibration are shown in Fig. 5. The nonlinear shear response of the material model is obtained by combining damage and friction (that occurs at the contact between mi-

Table 1. Mechanical properties used in the model of T700/E445 unidirectional composite.

Strength properties (MPa)	**Initial misalignment**	**Damage**
$X_T = 1920$	$\theta_i^{12} = 0.0°$	$p = -0.7$
$Y_T = 28$	$\theta_i^{13} = 3.0°$	$\gamma_f = 2.0$; $\gamma_L^{cr} = \gamma_L^{cr} = 0.12$
		$\tau_0 = 35$ (MPa)
	Friction properties	
Internal pressure (MPa)	Coefficient of friction	
$p_0 = 60$	$\mu = 0.4$	

crocrack surfaces). The inelastic behaviour (as well as hysteresis loops) are modelled using a stick/slip behaviour rather than by plasticity. By doing so, it is possible to account for material nonlinearity response in an efficient and physically based way.

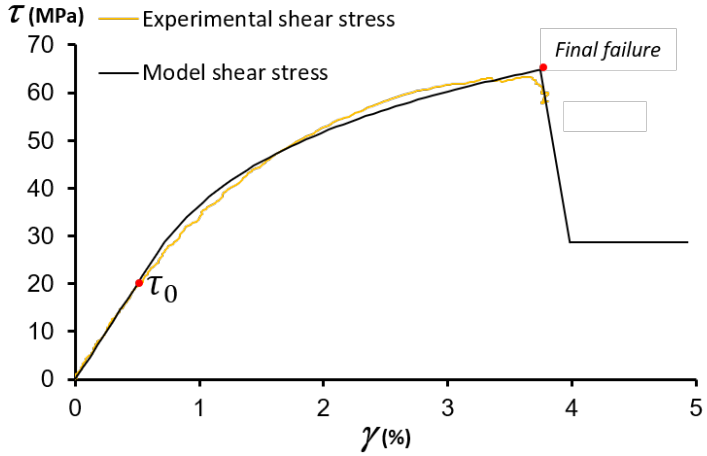

Figure 5. Shear calibration

3. Verification with a micromechanical model

A single finite element model of the current damage model was compared against a *computational micromechanics model* (CMM) developed in Abaqus.

The micromechanical 3D model consists of a single-fibre embedded in polymer matrix extruded along a sine curve which explicitly represents the initial misalignment of the fibre, φ_0, as shown in Fig. 6a. A cohesive damage model is defined at the fibre-matrix interface including friction, see yellow surface in Fig. 6b. The fibre is considered as a linear elastic transversely isotropic solid, and the polymer matrix takes into account plastic deformation, damage and

pressure sensitivity typical of polymers. A fully detailed description of this CMM model can be found in [15, 12].

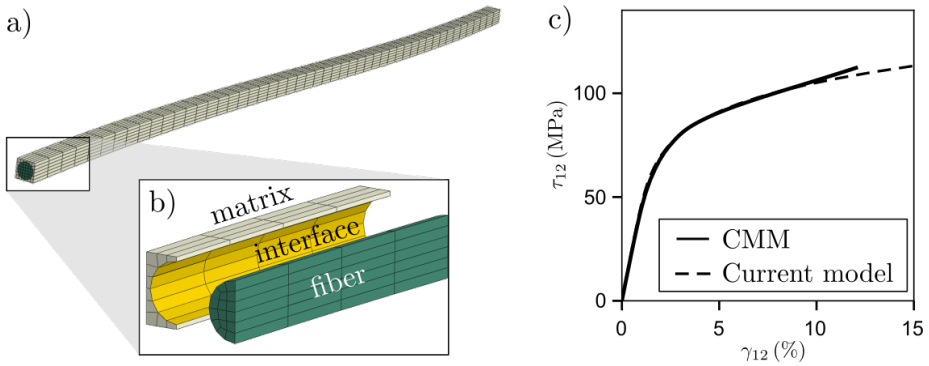

Figure 6. a) Micromechanical single-fibre 3D model, b) exploded half view of a detail of the mesh and constituents (fibre, matrix and interface), and c) in-plane shear curves of the CMM model and the current constitutive model presented in this work.

For the comparison with the CMM model, some of the parameters of the constitutive model presented in this work were fitted to reproduce the shear response of the material system AS4/8552 as illustrated in Fig. 6c. The final fitting was: $p = -0.65$, $\gamma_f = 2.0$, $\tau_0 = 50$ MPa, $p_0 = 30$ MPa. The stiffness in the longitudinal direction of the ply was estimated through the rule of mixtures assuming a fibre volume fraction of 60% ($E_1 = 137.1$ GPa). It should be noticed that, in the mesoscale constitutive model, eventual collapse of the ply was disabled to achieve a fair comparison with the CMM model.

The mechanical response under longitudinal compression is shown in Fig. 7a for four different initial misalignments ($\varphi_0 = 1.5,\ 2.5,\ 3$ and $4°$). Both models are able to capture the initial linear elastic stage up to the peak load (compressive strength, X_c) followed by a sudden load drop due to fibre kinking down to a residual crushing stress. Good agreement between the two models is observed during the elastic regime and up to the peak load when fibre kinking is triggered. This is clearly evidenced on the sensitivity curves in Fig. 7b, in which the maximum difference in the compressive strength for the range of initial misalignment considered is below 7%. The analytical estimation shown through the solid black line in Fig. 7b was obtained by applying the *fibre kinking theory* (FKT) originally proposed by [5] and later generalized by [16] into the LaRC04 failure criteria. However, a difference around 150 MPa is evidenced in the crushing stress obtained from the two models. This disagreement may be explained by the strategy followed to fit the parameters describing the current constitutive model by using just one characteristic curve of the material (in-plane shear, $\tau_{12} - \gamma_{12}$, see Fig. 6c), therefore lacking detailed characterization of the parameters ($p,\ \gamma_f,\ \tau_0,\ p_0$).

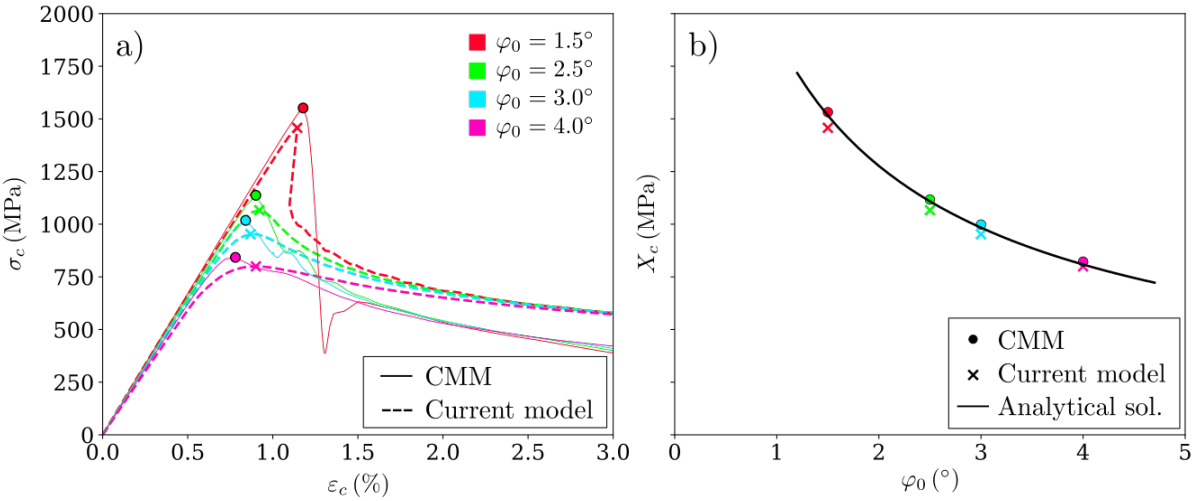

Figure 7. Comparison of the current constitutive model with the CMM under pure longitudinal compression for different initial misalignments φ_0: a) stress vs. strain curves and b) compressive strength vs. initial misalignment including the analytical solution from [5].

4. Verification at the specimen level

The verification of the model is done with the simulation of a simple flat specimen under three point bending. The dimensions are shown in Fig. 8 and the layup is $[90/0/(45/\text{-}45)_2/0/90]$ the material system is T700/E445.

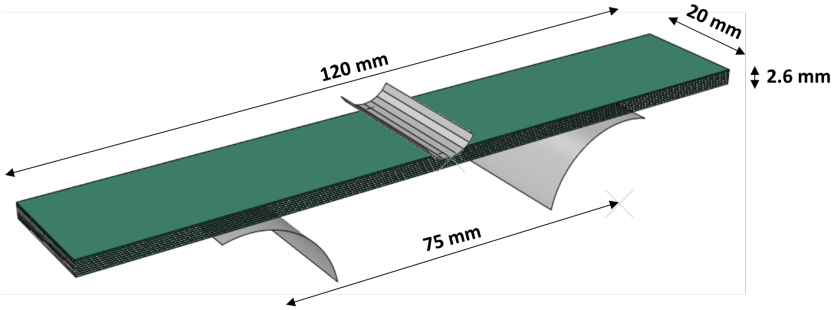

Figure 8. Representative image of the setup of the specimen loaded in three point bending

Two models with one element per ply were created and simulated using ABAQUS/Explicit 2019. For simplicity, no delaminations were considered at this stage. The element length was changed from 1 mm to 0.6 mm in order to test the mesh size sensitivity of the model. The average fibre misalignment considered was 3°. It is important to point out that this setup is not ideal for a more in-depth model validation due to the sudden nature of failure. Although

this setup fulfils the following purposes: (i) To verify the robustness of the modelling in a real simulation case; (ii) To check the sensitivity of the model to mesh refinement; (iii) To evaluate the performance of the model against experiments; (iv) Investigate the interaction of fibre kinking with matrix damage.

The model has run successfully without any nonphysically behaviour spotted throughout the simulation. Furthermore, the two different mesh yield very similar results as shown in Fig. 9. The results correlate well with experiments.

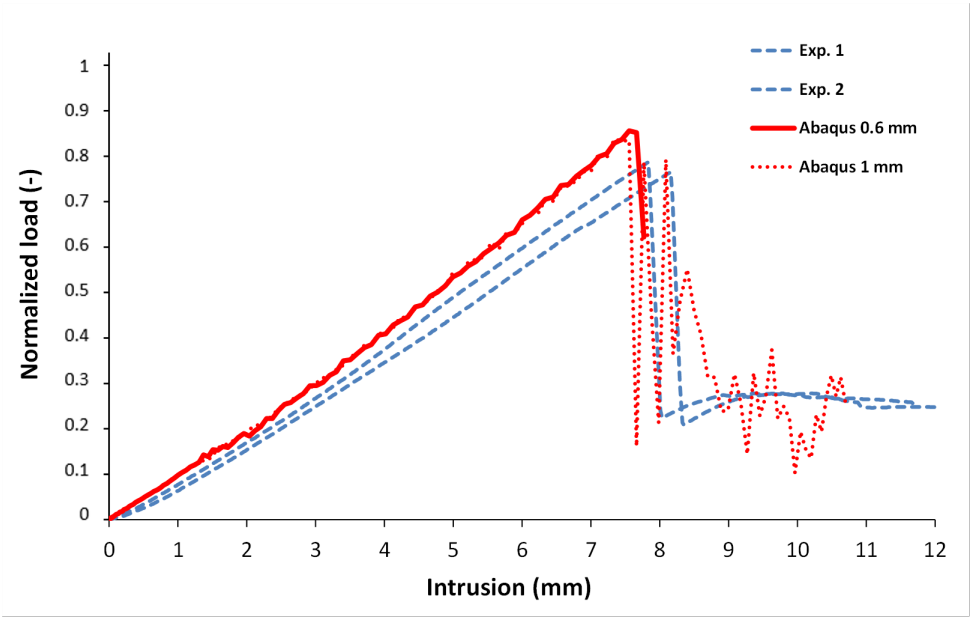

Figure 9. Experimental and numerical normalized load response vs. intrusion

In order to investigate the interaction between fibre kinking and matrix damage, the plots of the damage variable immediately before failure were investigated as shown in Fig. 10. Note that the only area with damage values close to one is loaded in transverse tension, which probably is not responsible to trigger failure. There is also no fibre damage in tension at this moment. Therefore, the catastrophic failure must have occurred due to an interaction between fibre compression and matrix damage. Since the model captured this sudden failure at the correct moment the interaction between fibre kinking and matrix damage looks meaningful.

5. Conclusions

A novel approach to model damage growth of composite is presented. Two previous models by two of the current authors are merged into the present unified model. The lack of separation of damage modes allows for better interaction and flexibility between modes which is fundamental for accuracy in multi-axial loading scenarios. The model is verified against micro-mechanical simulations with very similar results for stiffness, strength and crushing response. A

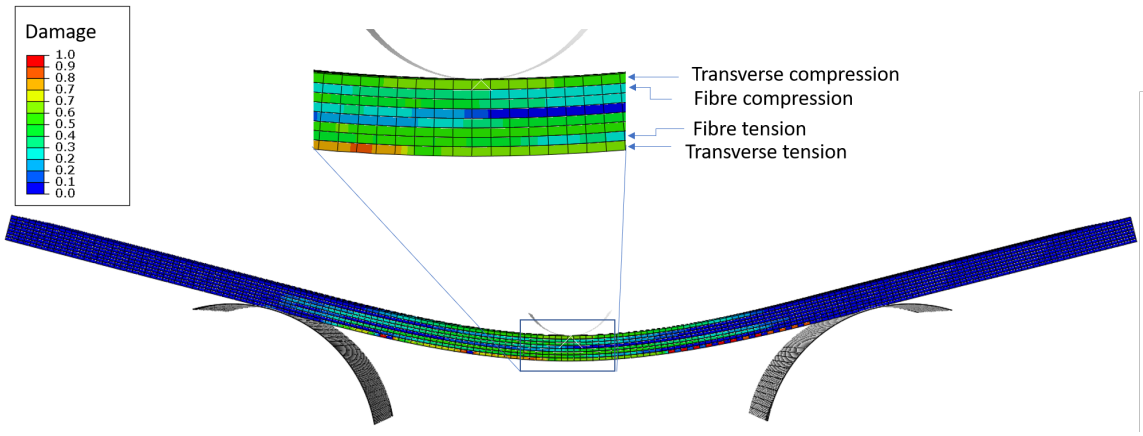

Figure 10. Damage contour before catastrophic failure occurs

verification at specimen level shows that the model has low mesh sensitivity and is able to predict catastrophic failure by interaction between fibre compression and matrix damage. Future work will focus on further validation at the material point and specimen level.

6. Acknowledgments

This work was been funded by energimyndigheten (Swedish Energy Agency), project number 50179-1; and co-funded from Gestamp Hardtech.

References

[1] F. Deleo, B. Wade, P. Feraboli et al. Crushing of composite structures: experiment and simulation. In: *Proceedings of the 50th AIAA/ASME/ASCE/AHS/ASC Structures, Structural Dynamics, and Materials Conference*, Palm Springs, CA, United States, 7 May 2009, 22p.

[2] A. C. Bergan. A Three-Dimensional Mesoscale Model for In-Plane and Out-of-Plane Fiber Kinking. In: *AIAA SciTech 2019 Forum*, San Diego, CA, United States, 7-11 January 2019.

[3] Z. Bažant and M. Jirásek. Nonlocal Integral Formulations of Plasticity and Damage: Survey of Progress. *Journal of Engineering Mechanics*, 128(11):1119–1149, 2002.

[4] T. Bru, R. Olsson, R. Gutkin, and G. M. Vyas. Use of the Iosipescu test for the identification of shear damage evolution laws of an orthotropic composite. *Composite Structures*, 174:319–328, 2017.

[5] B. Budiansky and N. Fleck. Compressive failure of fibre composites. *Journal of the Mechanics and Physics of Solids*, 41(1):183–211, 1993.

[6] L. N. S. Chiu, B. G. Falzon, R. Boman, B. Chen, and W. Yan. Finite element modelling of composite structures under crushing load. *Composite Structures*, 131:215–228, 2015.

[7] S. Costa, T. Bru, R. Olsson, and A. Portugal. Improvement and validation of a physically based model for the shear and transverse crushing of orthotropic composites. *Journal of Composite Materials*, 53(12):1681–1696, 2019.

[8] S. Costa, M. Fagerström, and R. Olsson. Development and validation of a finite deformation fibre kinking model for crushing of composites. *Composites Science and Technology*, 197:108236, 2020.

[9] S. Costa, R. Gutkin, and R. Olsson. Mesh objective implementation of a fibre kinking model for damage growth with friction. *Composite Structures*, 168:384–391, 2017.

[10] R. Gutkin, S. Costa, and R. Olsson. A physically based model for kink-band growth and longitudinal crushing of composites under 3D stress states accounting for friction. *Composites Science and Technology*, 135:39–45, 2016.

[11] R. Gutkin and S. T. Pinho. Combining damage and friction to model compressive damage growth in fibre-reinforced composites. *Journal of Composite Materials*, 49(20):2483–2495, 2015.

[12] G. C. Herraez M, Bergan AC. Modeling fiber kinking at the microscale and mesoscale. Technical Report TP–2018–220105, NASA, 2018.

[13] P. Maimí, P. Camanho, J. Mayugo, and C. Dávila. A continuum damage model for composite laminates: Part i – constitutive model. *Mechanics of Materials*, 39(10):897 – 908, 2007.

[14] C. McGregor, N. Zobeiry, R. Vaziri, A. Poursartip, and X. Xiao. Calibration and validation of a continuum damage mechanics model in aid of axial crush simulation of braided composite tubes. *Composites Part A: Applied Science and Manufacturing*, 95:208–219, 2017.

[15] F. Naya, M. Herráez, C. Lopes, C. González, S. Van der Veen, and F. Pons. Computational micromechanics of fiber kinking in unidirectional FRP under different environmental conditions. *Composites Science and Technology*, 144:26–35, May 2017.

[16] S. T. Pinho, C. G. Dávila, P. P. Camanho, L. Iannucci, and P. Robinson. Failure Models and Criteria for FRP Under In-Plane or Three-Dimensional Stress States Including Shear Non-Linearity. Technical Report February, NASA/TM-2005-213530, 2005.

[17] S. T. Pinho, L. Iannucci, and P. Robinson. Physically based failure models and criteria for laminated fibre-reinforced composites with emphasis on fibre kinking: Part I: Development. *Composites Part A: Applied Science and Manufacturing*, 185:774–785, 2006.

[18] S. T. Pinho, L. Iannucci, and P. Robinson. Physically based failure models and criteria for laminated fibre-reinforced composites with emphasis on fibre kinking. Part II: FE implementation. *Composites Part A: Applied Science and Manufacturing*, 37:766–777, 2006.

[19] W. Tan and B. G. Falzon. Modelling the crush behaviour of thermoplastic composites. *Composites Science and Technology*, 134:57–71, 2016.

[20] W. Tan, B. G. Falzon, and M. Price. Predicting the crushing behaviour of composite material using high-fidelity finite element modelling. *International Journal of Crashworthiness*, 20(1):60–77, 2015.